





Cite this: DOI: 10.1039/c9cp03155c

# Molecular dynamics study of natural rubber–fullerene composites: connecting microscopic properties to macroscopic behavior†

Wasinee Khuntawee,<sup>abc</sup> Thana Sutthibutpong,<sup>acd</sup> Saree Phongphanphanee,<sup>acef</sup>  
Mikko Karttunen <sup>ghi</sup> and Jirasak Wong-ekkabut <sup>\*abcf</sup>

Macroscopic and microscopic properties of fullerene (C<sub>60</sub>)–*cis*-polyisoprene (*cis*-PI) composites at varying fullerene concentrations were investigated using atomistic molecular dynamics (MD) simulations over microsecond time scales. Results show that the introduction of fullerenes into a polymer matrix increases density, bulk modulus and heat capacity while thermal expansivity decreases. The presence of fullerenes slowed the diffusion of both C<sub>60</sub> and *cis*-PI. Moreover, increasing fullerene concentration results in ordering of the *cis*-PI chains at the *cis*-PI–fullerene interfaces and shrinking of bulk PI regions. Free energy calculations of fullerene dimerization suggest that fullerenes disperse at low and aggregate at high fullerene concentrations. Our multi-scaled analysis approach demonstrates the role of ‘ordered’ regions adjacent to the interface between *cis*-PI and fullerene in controlling the level of order and mobility of the *cis*-PI chains. The relationship between the microscopic behavior and the changes in mechanical and thermal properties are discussed. Our study is beneficial for further studies and development of advanced rubber technology for novel, cost-effective, material with very high stiffness and thermal endurance with optimizing conditions of filler contents.

Received 4th June 2019,  
Accepted 21st August 2019

DOI: 10.1039/c9cp03155c

rsc.li/pccp

## 1. Introduction

Natural rubber (NR) mainly contains high molecular weight polymer with *cis*-1,4-polyisoprene (*cis*-PI) being the major component.<sup>1,2</sup> It is well-known that NR's low tensile strength,

low elasticity and low abrasion resistance restrict its practical applications.<sup>3</sup> On the other hand, advanced rubber-based materials are widely used in applications such as green energy tires,<sup>4,5</sup> high-performance plastics,<sup>6</sup> and structural parts of advanced equipment, *e.g.*, flexible sensors<sup>7</sup> and electrical insulators.<sup>8</sup> Rubber technology is continuously being developed not only to improve physical and mechanical properties but also to achieve green technology with low cost and uncomplicated laboratory procedures.<sup>9</sup>

The general technique to improve mechanical properties of pure NR is vulcanization in which crude NR is heated together with sulfur;<sup>10–12</sup> vulcanized NR is difficult to recycle because of sulfur cross-links.<sup>13,14</sup> Alternatively, the addition of fillers, such as carbon black (CB), to the NR matrix can enhance durability and elastic moduli of NR-based composites.<sup>15,16</sup> The strength of CB–NR composites is dramatically increased compared to vulcanized NR.<sup>17</sup> Moreover, the presence of CB in NR can be helpful for recycling of vulcanized NR by microwave technique;<sup>18</sup> microwave radiation is absorbed by CB resulting in the heating up of rubber composites which induces the devulcanization process.

Concentration and structure of CB have important roles in improving mechanical and dynamic properties of rubber composites.<sup>19,20</sup> The CB structure is formed by the agglomeration of aggregated CB particles *via* van der Waals interactions. The particle size, aggregate size and agglomerate size are specified for

<sup>a</sup> Computational Biomodelling Laboratory for Agricultural Science and Technology (CBLAST), Faculty of Science, Kasetsart University, Bangkok 10900, Thailand. E-mail: jirasak.w@ku.ac.th; Tel: +66-2562-5555 ext. 647335

<sup>b</sup> Department of Physics, Faculty of Science, Kasetsart University, Bangkok, 10900, Thailand

<sup>c</sup> Thailand Center of Excellence in Physics (ThEP Center), Commission on Higher Education, Bangkok 10400, Thailand

<sup>d</sup> Theoretical and Computational Science Center (TaCS), Science Laboratory Building, Faculty of Science, King Mongkut's University of Technology Thonburi (KMUTT), 126 Pracha-Uthit Road, Bang Mod, Thrung Khru, Bangkok 10140, Thailand

<sup>e</sup> Department of Material Science, Faculty of Science, Kasetsart University, Bangkok, 10900, Thailand

<sup>f</sup> Specialized Center of Rubber and Polymer Materials for Agriculture and Industry (RPM), Faculty of Science, Kasetsart University, Bangkok 10900, Thailand

<sup>g</sup> Department of Chemistry, The University of Western Ontario, 1151 Richmond Street, London, Ontario N6A 5B7, Canada

<sup>h</sup> Department of Applied Mathematics, The University of Western Ontario, 1151 Richmond Street, London, Ontario N6A 5B7, Canada

<sup>i</sup> The Centre of Advanced Materials and Biomaterials Research, The University of Western Ontario, 1151 Richmond Street, London, Ontario N6A 5B7, Canada

† Electronic supplementary information (ESI) available. See DOI: 10.1039/c9cp03155c

each type of CB.<sup>21</sup> Elongation modulus, hardness, tensile strength, tear strength, Payne effect and heat buildup are increased when the amount of CB increases (varied from 30 phr (parts per hundred rubber) to 70 phr)<sup>19</sup> with 60 phr being the suggested optimum. The high structure CB (the name stems from large number of CB particles per aggregate; low structure has small number of CB particles per aggregate) shows high tensile stress. In contrast, the stress of rubber composite with lower structure CB stress is reduced.<sup>20</sup> High CB concentrations and low structure CB cause fatigue cracks resulting from inhomogeneous dispersion of CB.<sup>22,23</sup> Thus, the dispersion of filler and the filler–filler interactions play a crucial role in determining the mechanical properties of NR composites.<sup>24</sup>

NR nanocomposites beyond CB are of great interest.<sup>25,26</sup> Filling the NR matrix with, *e.g.*, graphene, carbon nanotubes (CNT), or fullerene (C<sub>60</sub>), could provide reinforced NR composites.<sup>27</sup> For example, it has been shown that with 0.1–3 phr graphene (~10–20 nm), tensile strength increases by 14–33% in comparison with CB–NR nanocomposites.<sup>28</sup> Many studies have shown that multiwalled CNTs (MWCNT) dispersed homogeneously in an NR matrix improve mechanical properties:<sup>27,29,30</sup> hardness, tensile modulus and tensile strength have been shown increase with MWCNT concentrations of 2–8 phr.<sup>31</sup> Interestingly, the tensile strength of CNT–NR composites has been shown to decrease when the CNT concentration exceeds about 4 phr.<sup>31</sup> Thermal resistance increased by 30% for NR composites with 1 phr MWCNT, compared to NR without MWCNT at 200 °C.<sup>30</sup>

Among the carbon nanoparticle fillers, C<sub>60</sub> has been significantly less studied than the others. NR composites with C<sub>60</sub>-containing CB (0.065–0.75 phr C<sub>60</sub>) have been shown to increase rebound resilience elasticity (ISO 4662:1986),<sup>32</sup> hardness and tensile modulus with increasing amount of C<sub>60</sub>.<sup>33</sup> Interestingly, Al-Hartomy *et al.* have shown that the elongation modulus ( $M_{100}$ ) and hardness increase by 13–138% and 4–10%, respectively, when C<sub>60</sub> concentrations of 0.5–1.5 phr were added without CB.<sup>34</sup> However, there appears to be no studies of rubber composites with high C<sub>60</sub> concentrations (>40 phr, which is in the same range as the amount of CB filler in NR matrix). Al-Hartomy *et al.* studied the aggregation of C<sub>60</sub> particles at 0.5–1.5 phr by scanning electron microscopy (SEM) and transmission electron microscopy (TEM).<sup>34</sup> The SEM results showed aggregation of C<sub>60</sub> on surface with aggregate sizes in the range of 0.1–0.2 μm. In contrast, however, high-resolution TEM used in the same study suggested that the C<sub>60</sub> nanoparticles disperse and their aggregate sizes decrease to 40–50 nm. It should be noted that these experiments were limited to observations of morphology and behavior of C<sub>60</sub> at the microscopic level. Understanding of aggregation requires knowledge of the molecular-level interactions. Previous studies have suggested that a small amount of C<sub>60</sub> can enhance hardness, modulus and elasticity<sup>33,34</sup> and that degradation energies rubber network, friction coefficient and aging resistance increase with increasing C<sub>60</sub> concentration.<sup>33</sup> Consequently, it has been anticipated that C<sub>60</sub> in tread rubber could help to reduce tire temperatures. C<sub>60</sub> synthesis is, however, expensive but C<sub>60</sub> mixed with CB or mixtures C<sub>60</sub>/C<sub>70</sub> are potential alternatives for industrial polymer nanocomposites.<sup>33,35</sup>

In this study, C<sub>60</sub>–NR composites were investigated using MD simulations of *cis*-PI melts with 200 chains of 32-mers were with fullerene concentrations ranging from 0 to 64 phr. The effects of C<sub>60</sub> on structural, mechanical and thermal properties were analyzed. Aggregation of C<sub>60</sub> in the NR matrix was also studied and compared with free energy of fullerene dimerization. The aggregation of C<sub>60</sub> at high concentrations resulted in the confinement of *cis*-PI. It lead to shrinking and increase rigidity of the *cis*-PI chains. The bulk modulus and heat capacity were enhanced when C<sub>60</sub> was added. Heat capacity was reduced which is inversely correlated with the increase of bulk modulus. The ‘ordered’ region adjacent to the interface between *cis*-PI and fullerene decrease the mobility of the *cis*-PI chains. The C<sub>60</sub>–PI interactions might play a role in the enhancement of mechanical and thermal properties. Our results provide the relationship between microscopic and macroscopic properties and help to design advanced nanocomposite polymer materials.

## 2. Methodology

The united atom force field used here for *cis*-PI was previously developed and validated using Monte Carlo (MC) and MD simulations using *cis*-PI oligomer melts.<sup>36,37</sup> The intramolecular forces of *cis*-PI were modified based on the dynamic rotational isomeric state model.<sup>38,39</sup> Full structural details and interaction parameters are given in Table S1 (ESI†). MD simulations using the model for short chain *cis*-PI in melts have shown good agreement with experimental measurements for density, glass-transition temperature ( $T_g$ ), self-diffusion as well as thermal properties.<sup>36,37,40–42</sup> These simulations are also in good agreement with all-atom MD simulations using the OPLS (Optimized Potentials for Liquid Simulations) force field.<sup>42</sup>

Only a few simulations of rubber composites with carbon nanoparticles have been reported so far. In particular, atomistic and coarse-grained models of graphite–NR composites have been reported by Pandey *et al.*<sup>43</sup> Their results show that the PI chains lay down on the graphite surface and this consequently leads to slower dynamics of the PI chains compared to bulk. In addition, the MD simulations of He *et al.*<sup>44</sup> have shown the influence of CNT alignment on thermal conductivity of CNT–rubber composites. The thermal conductivity of the composite in the direction parallel to the CNT is over two orders of magnitude higher than in the transverse direction. In addition, enhanced thermal conductivity of CNT–polymers composites has been demonstrated.<sup>45,46</sup> It has been shown in a recent study that larger size and higher concentration of fullerene and graphene leads to a higher elastic modulus for their polyethylene composites.<sup>47</sup> When fullerene and graphene having approximately the same number of carbon atoms and the same concentration were added to polyethylene, the elastic modulus of the fullerene composite was higher.

### 2.1 MD simulations

The *cis*-PI–fullerene composites were studied with 9 different fullerene concentrations varying from 0.5 to 64 phr. The initial

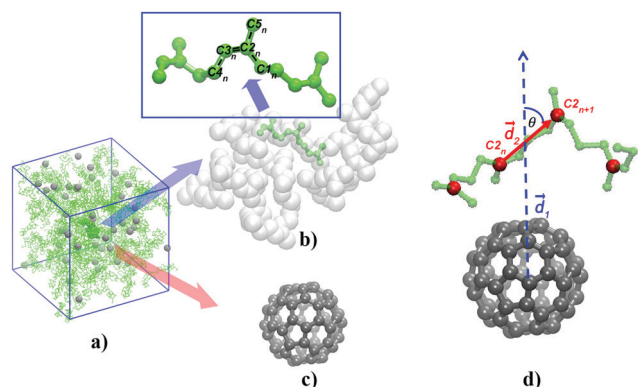


**Fig. 1** Initial structures used for rubber–fullerene composites in this study. The fullerene molecules ( $C_{60}$ , gray spheres) at various  $C_{60}$  concentrations (0–64 phr) were randomly added into *cis*-1,4-polyisoprene melt (green). a) Simulation boxes had 200 chains of 32-mer *cis*-1,4-polyisoprene and fullerene molecules (the number depending on concentration). b) The structure and essential nomenclature of *cis*-1,4-polyisoprene. The enlarged region shows three adjacent isoprene monomer units with *cis*-1,4-linkage. c) Atomic structure of  $C_{60}$  fullerene and d) a schematic diagram describing the distance between the center of mass (COM) of the  $C_{60}$  molecule and the C2 atoms of two adjacent isoprene monomers ( $d_1$ ). The orientation of *cis*-PI chains with respect to the  $C_{60}$  is defined as the angle ( $\theta$ ) between vectors  $\vec{d}_1$  and  $\vec{d}_2$  as shown. The C2 atoms of *cis*-PI are shown as red spheres.

structure consisted of 200 chains of 32-mer *cis*-PI molecules (Fig. 1). Fullerenes (shown in Fig. 1c) were randomly added in *cis*-PI melts with the numbers of 3, 5, 11, 21, 32, 43, 85, 171 and 341, corresponding to concentrations of 0.5, 1, 2, 4, 6, 8, 16, 32 and 64 phr, respectively. All simulations were performed using the Gromacs simulation package version 5.1.1.<sup>48</sup> After conjugate gradient energy minimization, MD simulations were performed in the *NPT* ensemble (constant particle number, pressure and temperature). Each of the systems was simulated for at least 5  $\mu$ s with time step of 2 fs, and data was collected every 2 ps. Equilibration was determined by monitoring the autocorrelation functions for the end-to-end distance and the radius of gyration tensor (see Fig. S1, ESI<sup>†</sup>). The last 1000 ns of the simulations were used for analysis. Periodic boundary conditions were applied in all directions. Isotropic pressure was maintained with the Parrinello–Rahman algorithm<sup>49</sup> at 1 bar with  $\tau = 1.0$  ps and compressibility =  $4.5 \times 10^{-5}$  bar<sup>-1</sup>. The temperature was controlled with the Parrinello–Donadio–Bussi velocity rescale (*v*-rescale) thermostat<sup>50</sup> at 300 K and time constant of  $\tau = 0.1$  ps. A cutoff radius of 1.0 nm was applied for real space part of electrostatic interactions and Lennard-Jones interactions. The effect of temperature on density and self-diffusion has been previously studied in MD simulations of *cis*-1,4-polyisoprene oligomer melts.<sup>36</sup> Density was observed to decrease and self-diffusion increase upon increasing temperature. In our study, the simulation temperature was set above the calculated glass transition temperature for 32-mer *cis*-PI,<sup>42</sup> and density comparable to the experimental density of a *cis*-PI melt. The particle-mesh Ewald (PME) method<sup>51–53</sup> was used for long-range electrostatic interactions with reciprocal-space interactions evaluated on a 0.12 nm grid and cubic interpolation of order four. All bond lengths were constrained with the P-LINCS algorithm.<sup>54</sup> The simulation parameters and protocols have been tested and

discussed in previous works.<sup>55–57</sup> List of systems and simulation times is provided in Table S2 (ESI<sup>†</sup>). All visualizations were done using the Visual Molecular Dynamics (VMD) software.<sup>58</sup>

## 2.2 Measuring the macroscopic and thermodynamic parameters

Variances and covariances of volume and enthalpy were used to calculate the bulk modulus ( $\kappa$ ), thermal expansion coefficient ( $\gamma$ ) and specific heat capacity ( $c_p$ ) using

$$\kappa = \frac{k_B T \langle V \rangle}{\langle V \rangle^2 - \langle V^2 \rangle} \quad (1)$$

$$\gamma = \frac{\langle VH \rangle - \langle V \rangle \langle H \rangle}{N_A k_B T^2 \langle V \rangle} \quad (2)$$

$$c_p = \frac{\langle H \rangle^2 - \langle H^2 \rangle}{m N_A k_B T^2}, \quad (3)$$

where  $N_A$  is the Avogadro number,  $k_B$  is the Boltzmann constant and  $m$  represents the total mass of the system in atomic mass units. The angular brackets indicate averaging over simulation time.  $\kappa$ ,  $c_p$  and  $\gamma$  values calculated for *cis*-PI in melts were used for validation against experimental results, while those for the *cis*-PI–fullerene composites were used to monitor macroscopic changes due to the addition of fullerene (see Results).

## 2.3 Pairwise and interfacial interactions

To elaborate the changes in the macroscopic properties of *cis*-PI–fullerene composites, interactions between fullerenes causing filler aggregation and interfacial interactions between fullerene and PI were analyzed at different fullerene concentrations. The radial distribution functions (RDF;  $g(r)$ ) of  $C_{60}$ – $C_{60}$  and  $C_{60}$ –PI were calculated and the potentials mean forces (PMF) were determined using<sup>59,60</sup>

$$\text{PMF} = -k_B T \ln(g(r)). \quad (4)$$

The peak values of PMF were used to justify preferences of  $C_{60}$  molecules for aggregation and PI chain adsorption. As PI conformations were more affected by nearby fullerenes, the distance between each pair of a C2 atom from an isoprene monomer and its closest fullerene was also determined. The probability distribution of the distance between each C2 atom and its closest fullerenes help to elucidate the amount of interfacial interactions between fullerene and PI chain. Additionally, the local density of the PI chains about a pair of aggregated and dispersed fullerene dimers were calculated to investigate the configuration of polymer chains around a fullerene pair, using our in-house Python scripts and the MDAnalysis library.<sup>61</sup>

## 2.4 PI chain parameter analysis

To validate the force field parameters, the end-to-end distance ( $R_0$ ) and the radius of gyration ( $R_g$ ) were calculated and compared to previous studies.<sup>42</sup> The ratio  $\langle R_g^2 \rangle / \langle R_0^2 \rangle$  was used to determine whether the polymers were random coils ( $\langle R_g^2 \rangle / \langle R_0^2 \rangle = 6$ <sup>62</sup>) or influenced by constraints. In addition, auto-correlation functions of  $R_0$  and  $R_g$  were used for determining

equilibration in all simulations (Fig. S1, ESI†). Mean square displacements (MSD) of the PI chains were calculated to assess the mobilities of polymer chains and compared with the MSDs calculated for fullerenes.

Chain ordering induced by fullerenes was examined by using the distance between the midpoint of two adjacent C2 atoms of *cis*-PI and the center of mass of a C<sub>60</sub> (*d*<sub>1</sub>) molecule as shown in Fig. 1d. The C2 atom was picked to represent each PI monomer because C2 is located closest to the COM of a monomer. The orientation angle  $\theta$  was determined by the vector  $\vec{d}_1$  from the fullerene center to the midpoint between the C2 atoms of the *n*th PI monomer and the (*n* + 1)th PI monomer, and vector  $\vec{d}_2$  from the C2 atom of the *n*th PI monomer to the C2 atom of the (*n* + 1)th PI monomer, (Fig. 1d). The order parameter is defined by

$$p = \left\langle \frac{3 \cos^2 \theta - 1}{2} \right\rangle \quad (5)$$

where the angular brackets indicate averaging over time.<sup>63</sup> The order parameter determines the orientational preferences for polymer chains relative to the radial vector  $\vec{d}_1$  (Fig. 1d):  $p = -0.5$  indicates that the polymer chains align perpendicular to  $\vec{d}_1$  and  $p = 1$  means that the population of polymer chains prefers to align parallel to  $\vec{d}_1$ . The value zero means that there is no preference for chain orientation and the system is in an amorphous state.

### 3. Results and discussions

#### 3.1 Global chain and macroscopic properties

**3.1.1 Bulk polyisoprene.** To assess equilibration, the auto-correlation function  $C(t)$  for the end-to-end distance ( $R_0$ ) and the radius of gyration ( $R_g$ ) were analyzed (Fig. S1, ESI†).  $R_g$  was computed using  $R_g = \sqrt{\lambda_1^2 + \lambda_2^2 + \lambda_3^2}$ , where  $\lambda_1^2$ ,  $\lambda_2^2$  and  $\lambda_3^2$

are the principal moments of the radius of gyration tensor and  $\lambda_1^2 \geq \lambda_2^2 \geq \lambda_3^2$ . The principal moments are related to the distribution of atoms and given by  $\sum_i (x_i - x_{\text{com}})^2$ ,  $\sum_i (y_i - y_{\text{com}})^2$  and  $\sum_i (z_i - z_{\text{com}})^2$ , where the subscripts *i* and com represent the *x*, *y* and *z* coordinates of atom *i* and the center of mass of the molecule, respectively. The relaxation times of  $R_0$  and  $R_g$  are reported in Table S3 (ESI†). In all cases, up to two hundred nanoseconds depending on fullerene concentrations was needed (autocorrelation functions are shown in Fig. S1, ESI†). Due to the long relaxation times, all simulations were performed for at least 5  $\mu\text{s}$  and the last 1  $\mu\text{s}$  of equilibrated configurations were used for analyses. We would like to mention, however, that although all simulations were performed over several microseconds the number of uncorrelated structures remains fairly small due to the long relaxation time. This is a general problem in simulations of rubber composites. Therefore, the structural, macroscopic and thermal properties of *cis*-PI melt were examined and compared to previous experiments and simulations in order to validate the use of the united-atom force field (Table S4, ESI†).

Initial and final structures of the simulations are shown in Fig. 2 and Fig. S2 (ESI†), and NR chain characteristics are provided in Table 1. The polymer expansion factor,  $\langle R_0^2 \rangle / \langle R_g^2 \rangle$ , was 6.20 suggesting random coil conformation.<sup>62</sup> It is in agreement with previous simulations by Sharma *et al.*,<sup>42</sup> who obtained 6.18 at the same degree of polymerization (32). The shape of NR chains was determined by asphericity defined as  $b = \lambda_1^2 - \frac{1}{2}(\lambda_2^2 + \lambda_3^2)$ . The value was found to be close to zero referring to a spherical shape (Table 1). Bulk density of 32-mer *cis*-PI was found to be  $854 \pm 2 \text{ kg m}^{-3}$  which is in the same range as experimental data ( $910 \text{ kg m}^{-3}$ )<sup>64</sup> and previous MD simulations (825, 840 and  $885 \text{ kg m}^{-3}$ , ref. 36, 43 and 42, respectively). The thermal expansion coefficient value of  $7.80 \pm 0.15 \times 10^{-4} \text{ K}^{-1}$  is also in good agreement with experimental

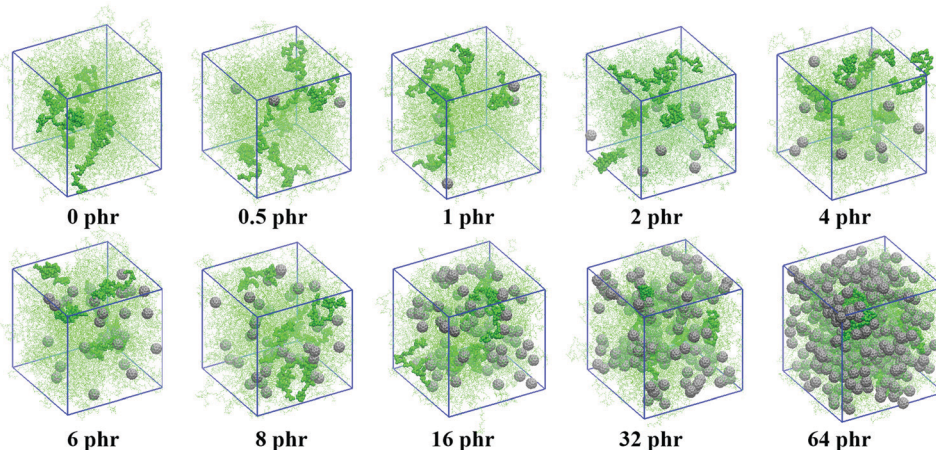


**Fig. 2** Snapshots of *cis*-PI–fullerene composites at C<sub>60</sub> concentrations of 0–64 phr showing the disaggregation and aggregation at low and high concentrations of C<sub>60</sub>, respectively. The gray and green represent C<sub>60</sub> and *cis*-PI, respectively. Some *cis*-PI chains are highlighted to illustrate the structural changes of *cis*-PI when C<sub>60</sub> concentration increases, *i.e.*, the *cis*-PI chains become extended and shrunken at low and high C<sub>60</sub> concentrations, respectively.

**Table 1** Structural measures of the NR chains at different  $C_{60}$  concentrations

$[C_{60}]$ (phr)	$\langle R_0^2 \rangle$ (nm <sup>2</sup> )	$\langle R_g^2 \rangle$ (nm <sup>2</sup> )	$\langle R_0^2 \rangle / \langle R_g^2 \rangle$	Asphericity
0	12.85 ± 0.41	2.07 ± 0.04	6.20	0.11 ± 0.03
0.5	12.31 ± 0.61	2.03 ± 0.05	6.06	0.10 ± 0.03
1	12.46 ± 0.56	2.03 ± 0.05	6.15	0.11 ± 0.03
2	12.71 ± 0.63	2.07 ± 0.06	6.14	0.08 ± 0.02
4	12.29 ± 0.48	2.00 ± 0.04	6.13	0.13 ± 0.04
6	12.41 ± 0.46	2.05 ± 0.03	6.05	0.09 ± 0.03
8	11.84 ± 0.39	1.99 ± 0.04	5.96	0.11 ± 0.02
16	11.85 ± 0.58	1.98 ± 0.03	5.99	0.08 ± 0.03
32	12.42 ± 0.34	2.00 ± 0.02	6.20	0.11 ± 0.02
64	7.63 ± 0.15	1.50 ± 0.01	5.09	0.09 ± 0.01

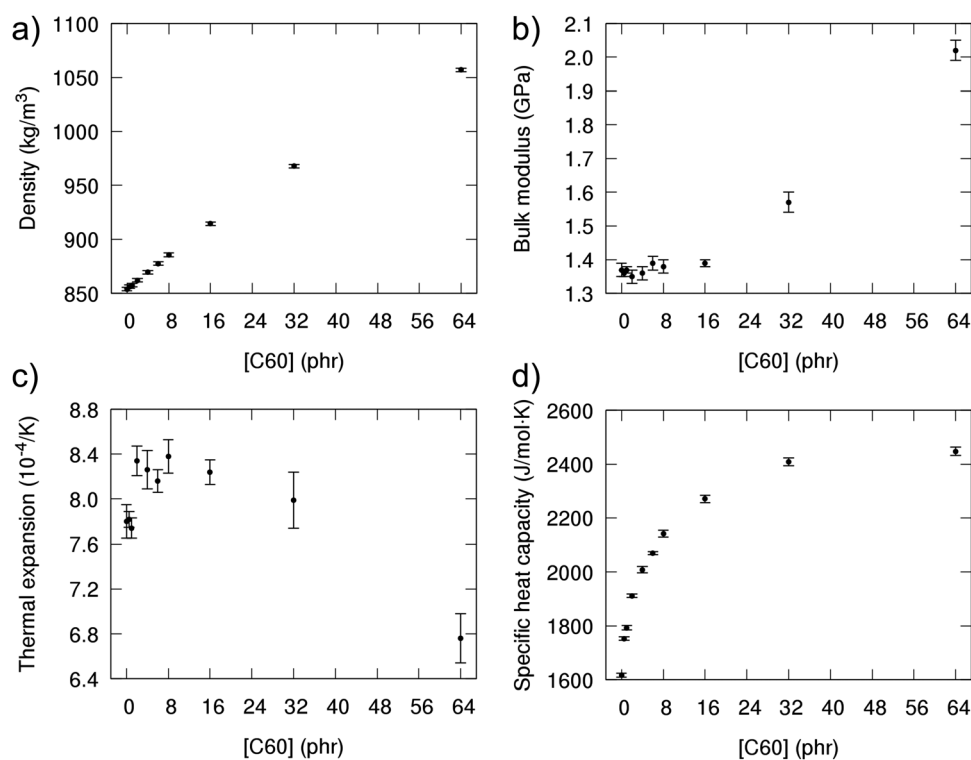
values of  $(6.7 \text{ to } 7.5) \times 10^{-4} \text{ K}^{-1}$ .<sup>65,66</sup> The bulk modulus (1.37 ± 0.02 GPa) was lower in comparison with previous simulations (1.95 GPa).<sup>42</sup>

**3.1.2 Effects of  $C_{60}$  concentrations on macroscopic properties: Different behaviors observed between high and low  $C_{60}$  concentrations.** Fig. 3a–d show the influence of  $C_{60}$  on macroscopic and thermal properties. Fig. 3a shows that the overall density of the composite increases almost linearly as a function of  $C_{60}$  concentration. The bulk moduli and the thermal volume expansion coefficients (Fig. 3b and c) were calculated from the fluctuations of the simulation box volumes and enthalpy, eqn (1) and (2). At  $[C_{60}] = 0.5\text{--}4.0$  phr, despite adding fullerene molecules into the *cis*-PI in melts, the bulk moduli of *cis*-PI–fullerene composites decreased slightly (less than 3%) below the bulk moduli of *cis*-PI melts (Fig. 3b). Bulk modulus starts to

increase slowly when increasing  $[C_{60}]$  from 4 to 16 phr. This is followed by a strong linear increase starting at 16 phr.

The thermal expansion coefficient is shown in Fig. 3c. There are no significant changes for  $[C_{60}]$  less than 1 phr and it increases for 2–8 phr after which it starts to decrease by 13% at 64 phr, compared with bulk NR. The thermal expansion coefficient of  $C_{60}$  is about an order of magnitude larger than that of bulk NR (the experimental value for  $C_{60}$  is  $6.2 \times 10^{-5} \text{ K}^{-1}$ ).<sup>67</sup> Thus, adding  $C_{60}$  to an NR composite should then lead to a linear increase in expansivity. This trend was observed for  $[C_{60}] \leq 32$  phr. The increase of thermal expansion in composites had been found in the previous MD simulation of polymer–CNT composite.<sup>68</sup> As for the specific heat, Fig. 3d, rapid increase was observed at  $[C_{60}] = 0\text{--}8$  phr (31–272  $\text{J kg}^{-1} \text{ K}^{-1}$  per 1 phr) followed by slower increase above 8 phr (1–16  $\text{J kg}^{-1} \text{ K}^{-1}$  per 1 phr).

An X-ray diffraction study by Alekseeva *et al.*<sup>69</sup> has shown that thermal properties of fullerene and polystyrene composites depend on fullerene concentration, and competition between plasticizing effects of fullerene and fullerene–polymer interactions. Plasticizing effects dominate at small fullerene concentrations, resulting in a disordered phase created by replacing a portion of the NR matrix by fullerenes and the loss in bulk modulus. On the other hand, interactions between fullerene and polymer molecules become more evident at high fullerene concentrations when the polymer chains become more ordered.<sup>69</sup> Molecular mechanisms of these effects are needed.

**Fig. 3** Effect of  $C_{60}$  as a function of the amount of  $C_{60}$  on a) density, b) bulk modulus, c) thermal expansion and d) specific heat capacity of *cis*-PI–fullerene composites.

### 3.2 Microscopic views: dynamic behavior, *cis*-PI structure and C<sub>60</sub>-C<sub>60</sub> interactions at different concentrations

**3.2.1 C<sub>60</sub>-C<sub>60</sub> interactions.** To investigate the thermodynamics of C<sub>60</sub> aggregation, the free energy of C<sub>60</sub> dimerization in *cis*-PI-C<sub>60</sub> composites was computed at different C<sub>60</sub> concentrations. The PMF profiles were calculated from the radial distribution function (RDF) profiles using eqn (4). The results are shown in Fig. 4a. The PMF profiles in *cis*-PI-C<sub>60</sub> composites are qualitatively similar to those measured in octane and lipid bilayers,<sup>70</sup> that is, two nearest neighbor shells within 2 nm are present in all profiles. The first nearest neighbor RDF shell of fullerenes about a reference fullerene was indicated by the first local minima of PMF profiles and were approximately 1 nm, while the second RDF shell and the second local minimum of PMF indicated that the second closest distance between the neighboring fullerenes became 1.4 nm.

Local distribution of *cis*-PI monomers about a fullerene pair was analyzed using our in-house python script (Fig. 5a). For each fullerene pair separated by a given distance, a coordinate transformation was done to place the two fullerenes on either side of the longitudinal axis in a cylindrical coordinate system. Then, the probability distribution of the C2 atoms of the PI chains as a function of radial and longitudinal coordinates was obtained by counting the number of C2 atoms within the grid-boxes. The product between the 2D probability map and the bulk density provides the local density as a function of the

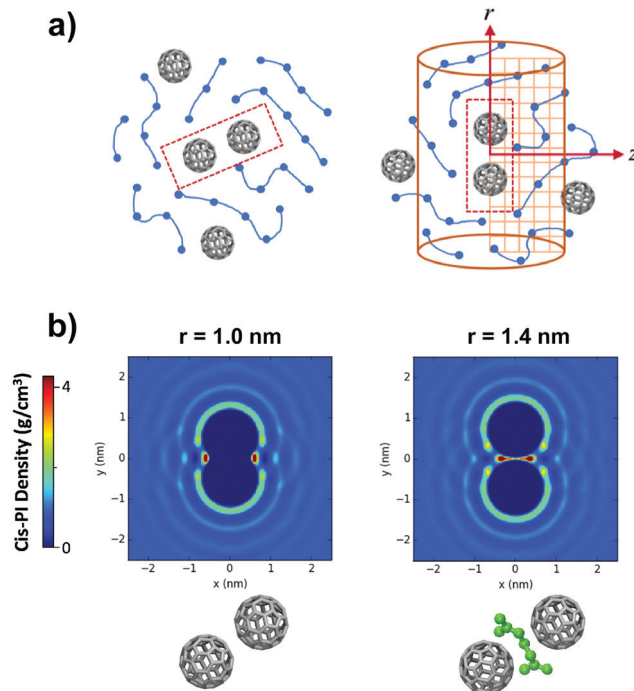


Fig. 5 a) Description of local distribution analysis of *cis*-PI monomers about a fullerene pair determined from a plane crossing the center of mass the fullerenes placed along the *y*-axis. b) Local density maps of *cis*-PI at fullerene separation distances of  $1.0 \pm 0.1$  nm and  $1.4 \pm 0.1$  nm corresponding to the first and the second RDF shell, respectively. The snapshots at each fullerene separation distance are enclosed with density map.

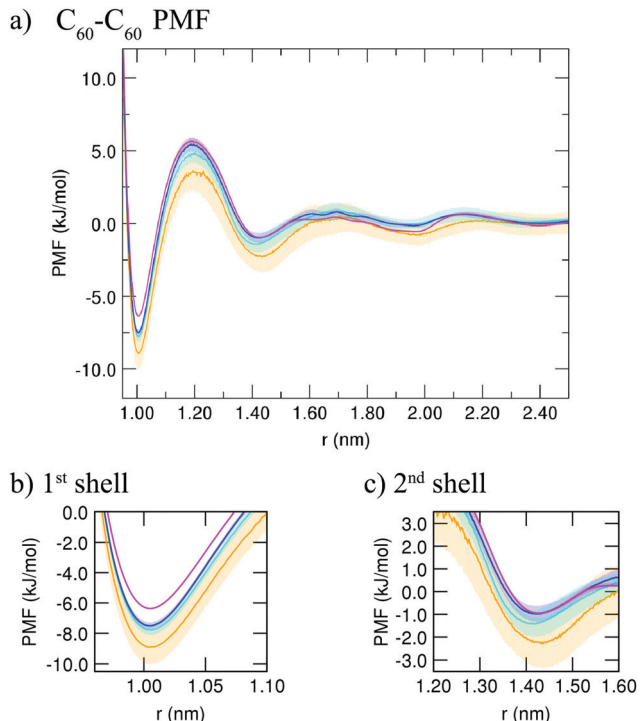


Fig. 4 a) The PMF of C<sub>60</sub>-C<sub>60</sub> interactions within the *cis*-PI-C<sub>60</sub> composites at 4–64 phr of [C<sub>60</sub>]. The PMF was set to zero at  $r = 3.0$  nm. (b and c) Present a close-up view of the first and second nearest neighbor shell, respectively. The free energies in first shell were lower than ones in the second shell suggesting dimerization of C<sub>60</sub> molecules.

radial and longitudinal coordinates and fullerene separation. Distribution of polyisoprene about a fullerene pair at separation distances  $1.0 \pm 0.1$  nm of the first RDF shell radius and  $1.4 \pm 0.1$  nm of the second RDF shell radius are displayed in Fig. 5a and b, respectively. No polyisoprene was found between the fullerene pair separated by  $1.0 \pm 0.1$  nm (first RDF shell), signifying aggregation of the fullerene pair. At separation distance  $1.4 \pm 0.1$  nm (second RDF shell), high polyisoprene density was observed between fullerenes, signifying dispersion of the fullerene pair as a polyisoprene chain was present between the fullerene pair.

At all concentrations, the first PMF minimum was found to be lower than the second one, suggesting that fullerenes aggregate rather than disperse. The first PMF minima of the *cis*-PI-C<sub>60</sub> at 4–32 phr [C<sub>60</sub>] were found between  $-7.0$  kJ mol<sup>-1</sup> and  $-9.0$  kJ mol<sup>-1</sup>. Surprisingly, the first minimum at 64 phr was found at  $-6.38 \pm 0.03$  kJ mol<sup>-1</sup>, showing less C<sub>60</sub>-C<sub>60</sub> pairwise binding preference than that of simulations with lower C<sub>60</sub> concentrations that contained smaller C<sub>60</sub> aggregated clusters. However, the coordination numbers of C<sub>60</sub> molecules about a reference C<sub>60</sub> molecule within the 1st shell distance ( $< 1.2$  nm) were still in good agreement with macroscopic properties (see Fig. 6). At C<sub>60</sub> concentrations of 32 and 64 phr, where the abrupt transitions in bulk modulus and thermal expansivity were observed within the simulations, the coordination number became greater than 1. It can be inferred that, when each of C<sub>60</sub> molecules within an NR matrix was

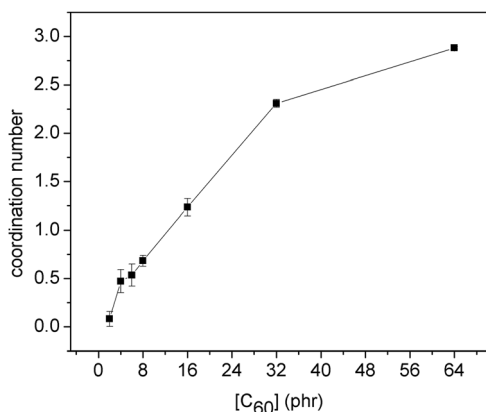


Fig. 6 The coordination numbers of  $C_{60}$  molecules as a function of concentration (that is, other  $C_{60}$  molecules within the 1st shell ( $<1.2$  nm)).

occupied with at least one other  $C_{60}$  molecule on average, changes in some macroscopic properties *e.g.*, bulk modulus and thermal expansivity were detected.

**3.2.2 Dynamic behavior of *cis*-PI and  $C_{60}$ : low chain mobility at the aggregated phase.** Diffusion coefficients ( $D$ ) of the *cis*-PI chains and  $C_{60}$  molecules in melts and composites at different  $C_{60}$  concentrations were estimated using the Einstein relation, calculated from the slope of the mean squared displacement (MSD)

$$\text{MSD} = \langle r^2 \rangle \sim 6Dt, \quad (6)$$

where  $D$  is the diffusion coefficient and  $t$  is time.

Table 2 presents the results calculated by fitting the MSD every 100 ns for the last 500 ns. The MSD plots of *cis*-PI and  $C_{60}$  are shown in Fig. S3 (ESI<sup>†</sup>). The diffusion coefficient of *cis*-PI in melt was determined to be  $2.4 \times 10^{-8} \text{ cm}^2 \text{ s}^{-1}$  which is of the same order of magnitude as the one determined experimentally by von Meerwall who found it to be about  $1.3 \times 10^{-8} \text{ cm}^2 \text{ s}^{-1}$  using pulsed-gradient spin-echo technique at 296 K for *cis*-PI of molar mass 1260 Da.<sup>71</sup> The self-diffusion increased by 2.5 orders of magnitude when temperature increased from 296 to 373 K and with *cis*-PI chain extension (molecular weight range 411 to 10 500 Da).<sup>71</sup> The presence of  $C_{60}$  in the *cis*-PI matrix resulted in an extreme decrease of *cis*-PI diffusion by 86% at 64 phr, compared to *cis*-PI in melts. Similarly, diffusion of  $C_{60}$  decreased significantly by over one order of magnitude when  $C_{60}$  concentration increased to 64 phr. The decrease of  $C_{60}$

Table 2 Diffusion coefficients ( $D$ ) of *cis*-PI and  $C_{60}$  in *cis*-PI- $C_{60}$  composites at 300 K

[ $C_{60}$ ] (phr)	$D$ [ <i>cis</i> -PI] ( $10^{-9} \text{ cm}^2 \text{ s}^{-1}$ )	$D$ [ $C_{60}$ ] ( $10^{-9} \text{ cm}^2 \text{ s}^{-1}$ )
0	$23.66 \pm 0.89$	—
0.5	$22.24 \pm 1.30$	$21.94 \pm 11.24$
1	$22.82 \pm 1.39$	$20.14 \pm 7.58$
2	$21.17 \pm 1.30$	$18.48 \pm 3.38$
4	$20.52 \pm 1.06$	$12.62 \pm 3.14$
6	$18.52 \pm 0.42$	$11.81 \pm 2.48$
8	$16.83 \pm 1.10$	$12.25 \pm 2.65$
16	$14.00 \pm 0.88$	$6.80 \pm 0.97$
32	$8.24 \pm 0.62$	$2.20 \pm 0.22$
64	$2.88 \pm 0.21$	$0.39 \pm 0.04$

diffusion at high concentrations has also been found in simulations of  $C_{60}$  in lipid membranes.<sup>72,73</sup> The diffusion coefficient of  $C_{60}$  in *cis*-PI was of the same order of magnitude as  $C_{60}$  diffusion in heterojunction polymer solar cells (*i.e.*, poly-3-hexylthiophene; P3HT);<sup>74</sup> the  $\pi$ - $\pi$  interactions of  $C_{60}$  with the thiophene rings of P3HT contributed to the diminished diffusion of  $C_{60}$ .<sup>74</sup> Moreover, localized  $C_{60}$  inducing an increase of lipid chain order has been reported.<sup>73</sup> The decrease of  $C_{60}$  and *cis*-PI diffusion with increasing  $C_{60}$  concentration corresponds to enhancement of bulk modulus of *cis*-PI composite with  $C_{60}$ . The influence of  $C_{60}$  on the chain order of *cis*-PI as well as on the  $C_{60}$ - $C_{60}$  interactions will be examined in Section 3.2.3.

### 3.2.3 Chain order and distribution at the PI- $C_{60}$ interface.

Interfacial interactions between  $C_{60}$  and *cis*-PI were investigated by measuring the radial distribution function (RDF) between the center of mass of a reference  $C_{60}$  molecule and the C2 atom of a reference *cis*-PI monomer (Fig. 7a). The first RDF peak at the distance 0.77 nm between the center of mass of a fullerene and the C2 atom shows that the density of PI in the first shell becomes more than twice the bulk density and significantly higher than that of the second shell at the  $C_{60}$ -PI distance of 1.23 nm, suggesting that PI polymers prefer binding to the spherical surface of a  $C_{60}$  molecule at all  $C_{60}$  concentrations. PMF profiles were calculated from the RDFs using eqn (4) and the first minimum ranged between  $-1.9$  and  $-2.2 \text{ kJ mol}^{-1}$ , while the second minimum was found between  $-0.60$  and  $-0.84 \text{ kJ mol}^{-1}$  (Fig. 7b) suggesting that the interfacial interactions between PI chains and fullerene were more favorable than interactions between PI chains themselves.

Conformations of PI polymers at fullerene interfaces are further elucidated by measuring the order parameter of PI-chain orientation relative to the radial vector from the center of mass of a fullerene to a short PI segment (eqn (5)). Time-averaged order parameter profiles for all simulations with 0.5–64 phr shown in Fig. 7c display similar behavior; the largest negative values of averaged order parameters of around  $-0.47$  were measured at the fullerene surface with the distance  $r = 0.7$  nm from the fullerene center of mass. The negative values of averaged order parameters suggest that PI chains have a higher tendency to orient in parallel with the fullerene surfaces. At further distance  $r$  from the fullerene center, positive peaks of averaged order parameters were observed at the middle between  $n$ th and  $(n + 1)$ th RDF shells, representing a higher tendency for polymer chains to orient perpendicular to fullerene surfaces. Meanwhile, negative peaks of averaged order parameters were observed at  $n$ th RDF shells, representing a higher tendency for polymer chains to orient perpendicular to fullerene surfaces. Similar to RDF and PMF profiles, the alternating pattern between positive and negative order parameters vanished with very long distance  $r$  from the center of reference fullerene, as the distribution of PI around a fullerene became uniform and no chain orientation preference was observed and PI became relatively amorphous.

Higher fullerene concentration reduced spaces between fullerene molecules, causing higher population of PI monomers to reside in close proximity to a fullerene molecule, as previously

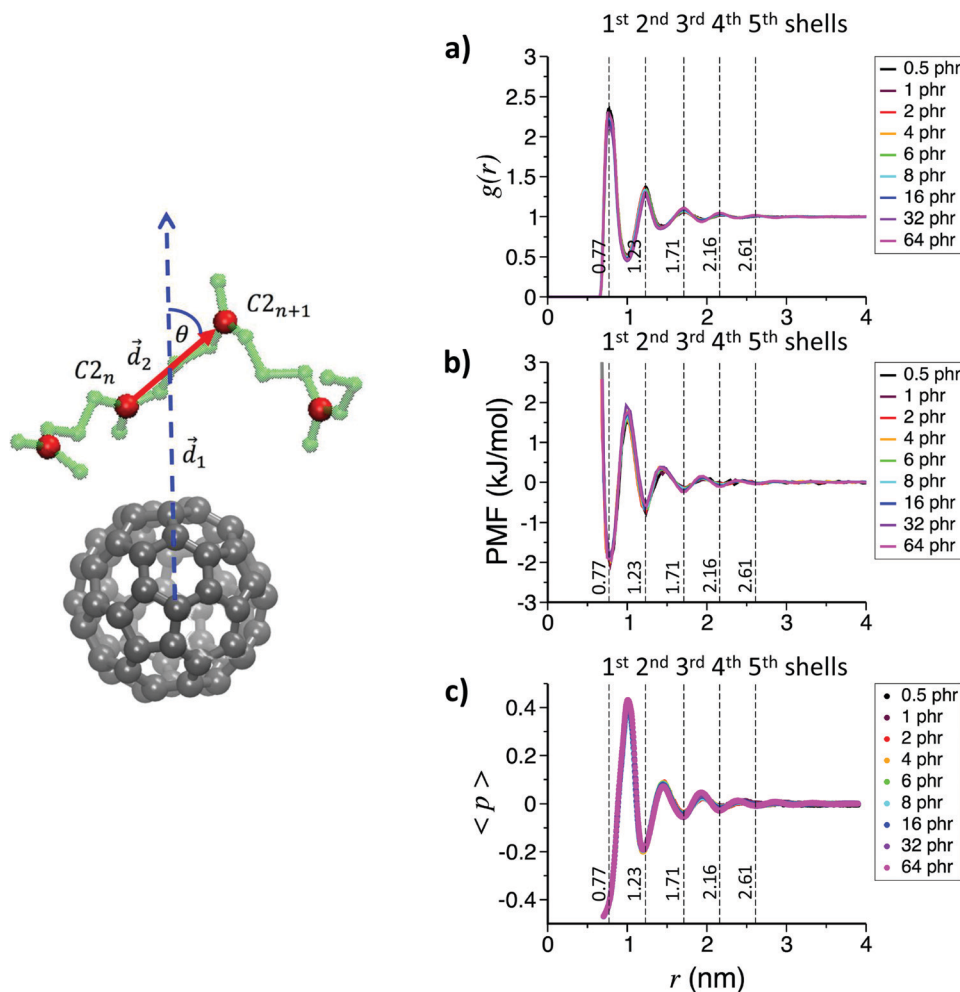
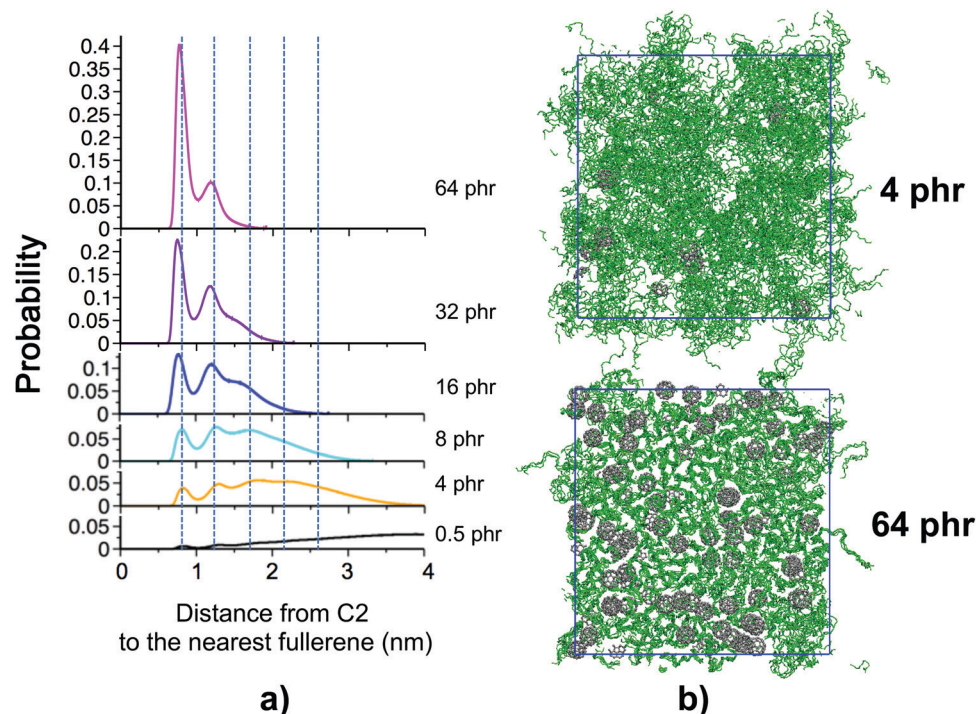


Fig. 7 a) Radial distribution functions between C2 atoms within the PI chains and the centers of masses of fullerenes calculated from the simulations of  $C_{60}$ -PI composites at  $[C_{60}] = 0.5$ –64 phr. b) The corresponding potential of mean force (PMF) between the C2 atoms and the fullerenes as a function of the distance between the C2 atom and fullerenes, and c) the order parameter (eqn (5)) calculated from the orientation angle  $\theta$  made by the vector  $\vec{d}_2$  from the C<sub>2</sub> atoms of a PI monomer  $n$  ( $C_{2n}$ ) to its adjacent PI monomer  $n + 1$  ( $C_{2n+1}$ ), and the vector  $\vec{d}_1$  from the fullerene center of mass to the center of mass between  $C_{2n}$  and  $C_{2n+1}$  within the simulations of  $C_{60}$ -PI composites at  $[C_{60}] = 0.5$ –64 phr. 1st–5th peak positions of RDF shells at  $C_{60}$ -PI distances 0.77 nm, 1.23 nm, 1.71 nm, 2.16 nm and 2.61 nm are represented by dashed lines.

seen in RDF profiles for the pairwise  $C_{60}$ -PI interactions. Fig. 8a displays the probability distributions of the distance between a PI monomer and the closest fullerene molecule for simulations at varied fullerene concentrations. The C<sub>2</sub> atom of each PI monomer was picked as the reference but only the distance from each C<sub>2</sub> atom to the center of mass of its closest fullerene was used, instead of the distances from all fullerene molecules as in the RDF profiles. The probability distributions shown in Fig. 8a were compared to 1st–5th peak positions from RDF indicated by dashed lines. 1st and 2nd local maxima of the probability profiles located at 1st and 2nd RDF peaks were found increasing with  $C_{60}$  concentrations. At low fullerene concentrations ( $< 16$  phr), 1st probability peaks were found lower than 2nd probability peaks, reflecting the low amount of interfacial interactions between PI monomers and  $C_{60}$ . As a result, the PI polymer chain network was completely amorphous, as shown in the superimposed snapshots taken from

the simulation at 4 phr (Fig. 8b). At high fullerene concentrations ( $\geq 16$  phr), the 1st probability peaks became higher than the 2nd probability peaks, suggesting the larger amount of interfacial interactions between PI monomers and fullerenes. Considering the higher peaks of order parameters at closer RDF peaks, the amount of ordered PI segments affected by fullerenes was increased with  $C_{60}$  concentration. At 64 phr, all PI monomers resided within either the 1st or the 2nd RDF shell of their closest fullerene. The superimposed snapshots of PI polymer chain network within a thin slab taken from the simulation at 64 phr (Fig. 8b) displayed a semi-crystalline structure as the high and low density regions were clearly distinguished. These results demonstrated the higher ordering and lower mobility of PI polymer chains induced by interfacial interactions between fullerene and PI polymer and the confinement effect introduced by high fullerene filler concentration.





**Fig. 8** a) The probability distributions of the distances between C2 atoms of *cis*-PI and their closest  $C_{60}$  molecules at concentrations of 0.5, 4, 8, 16, 32 and 64 phr. The 1st–5th peak positions of the RDF shells at fullerene–PI distances of 0.77 nm, 1.23 nm, 1.71 nm, 2.16 nm and 2.61 nm are represented by dashed lines. b) Five superimposed snapshots taken every 100 ps from a slab of 2 nm thickness within the equilibrated MD trajectory of  $C_{60}$ –PI composite at (top) 4 phr and (bottom) 64 phr.

## 4. Conclusion

Microscopic and macroscopic properties of *cis*-PI- $C_{60}$  composites at different  $C_{60}$  concentrations (0, 0.5, 1, 2, 4, 6, 8, 16, 32 and 64 phr) were explored using atomistic MD simulations. The concentration dependence of bulk and thermal properties of *cis*-PI- $C_{60}$  composites was studied with systems consisting of 200 chains of 32-mer *cis*-PI and  $C_{60}$  molecules. The density, bulk modulus and heat capacity of *cis*-PI- $C_{60}$  composites increase dramatically increased by 24%, 47% and 51%, respectively compared to *cis*-PI melts at 64 phr. In contrast, thermal expansion of *cis*-PI- $C_{60}$  composites decreased with increasing the  $C_{60}$  concentration. These are excellent characters of polymer composites which would provide low thermal expansion and high thermal conductivity.<sup>75</sup>

The plasticizing effect was observed in the bulk modulus of *cis*-PI- $C_{60}$  composites as they decreased at low  $[C_{60}]$  (4 phr). The mechanism of how  $C_{60}$  improves the macroscopic of *cis*-PI was taken into account by investigating the microscopic properties. The dispersion of  $C_{60}$  in the *cis*-PI matrix including the interaction of  $C_{60}$  itself and with *cis*-PI was the main contribution of the mechanical enhancement of polymer composites. At low  $C_{60}$  concentrations,  $C_{60}$  preferred to form the dispersed monomeric  $C_{60}$  in *cis*-PI. Meanwhile, aggregations of  $C_{60}$  were profound at high  $C_{60}$  concentration. The dimerization free energy of  $C_{60}$  strongly agreed with the  $C_{60}$  clustering fraction. Interestingly, contact between *cis*-PI and  $C_{60}$  increased the chain order of the *cis*-PI chain. Consequently, diffusion of both

$C_{60}$  and *cis*-PI decreased when  $[C_{60}]$  increased. This is due to  $C_{60}$  aggregation and lesser flexibility of the *cis*-PI chains. These dynamic changes correspond to the bulk modulus enhancement at high  $C_{60}$  concentrations. We envision our findings to be important in design of lightweight reinforcing rubber materials with thermal property improvements as well as for exotic rubber materials *e.g.*, thermally conductive rubber. It would also be interesting to study NR composites at very low  $C_{60}$  concentrations ( $<4$  phr) aiming to explore plasticizing effect of  $C_{60}$ –NR composites in future work.

## Conflicts of interest

The authors declare no competing financial interest.

## Acknowledgements

This work was financially supported by Kasetsart University Research and Development Institute (KURDI) and Faculty of Science at Kasetsart University (JW). The Thailand Research Fund (TRF) through the TRF Research Scholar (Grant No. RSA6180021) JW is acknowledged. TS thanks the Theoretical and Computational Science (TaCS) Center under Computational and Applied Science for Smart Innovation Research Cluster (CLASSIC), Faculty of Science, KMUTT. MK thanks the Natural Sciences and Engineering Research Council of Canada (NSERC) and the Canada Research Chairs Program. Computing facilities

were provided by SHARCNET (www.sharcnet.ca), Compute Canada (www.computecanada.ca) and the Department of Physics, Faculty of Science, Kasetsart University.

## References

- 1 T. Kakubo, A. Matsuura, S. Kawahara and Y. Tanaka, *Rubber Chem. Technol.*, 1998, **71**, 70–75.
- 2 A. P. Singh, S. G. Wi, G. C. Chung, Y. S. Kim and H. Kang, *J. Exp. Bot.*, 2003, **54**, 985–992.
- 3 F. Findik, R. Yilmaz and T. Köksal, *Mater. Des.*, 2004, **25**, 269–276.
- 4 P. Zhang, M. Morris and D. Doshi, *Rubber Chem. Technol.*, 2016, **89**, 79–116.
- 5 M.-J. Wang, P. Zhang and K. Mahmud, *Rubber Chem. Technol.*, 2001, **74**, 124–137.
- 6 I. Kong, S. Hj Ahmad, M. Hj Abdullah, D. Hui, A. Nazlim Yusoff and D. Puryanti, *J. Magn. Magn. Mater.*, 2010, **322**, 3401–3409.
- 7 S. C. B. Mannsfeld, B. C. K. Tee, R. M. Stoltenberg, C. V. H. H. Chen, S. Barman, B. V. O. Muir, A. N. Sokolov, C. Reese and Z. Bao, *Nat. Mater.*, 2010, **9**, 859–864.
- 8 T. Tanaka, G. C. Montanari and R. Mulhaupt, *IEEE Trans. Dielectr. Electr. Insul.*, 2004, **11**, 763–784.
- 9 S. Kohjiya, K. Murakami, S. Iio, T. Tanahashi and Y. Ikeda, *Rubber Chem. Technol.*, 2001, **74**, 16–27.
- 10 A. S. Aprem, K. Joseph and S. Thomas, *Rubber Chem. Technol.*, 2005, **78**, 458–488.
- 11 L. F. Li, Y. N. Bai, M. Lei and L. Liu, *Prog. Chem.*, 2015, **27**, 1500–1508.
- 12 J. Kruzalak, R. Sykora and I. Hudec, *Chem. Pap.*, 2016, **70**, 1533–1555.
- 13 M. Myhre and D. A. MacKillop, *Rubber Chem. Technol.*, 2002, **75**, 429–474.
- 14 J. Hopewell, R. Dvorak and E. Kosior, *Philos. Trans. R. Soc., B*, 2009, **364**, 2115–2126.
- 15 G. Heinrich, M. Klüppel and T. A. Vilgis, *Curr. Opin. Solid State Mater. Sci.*, 2002, **6**, 195–203.
- 16 D. G. Hundiwale, U. R. Kapadi, M. C. Desai and S. H. Bidkar, *J. Appl. Polym. Sci.*, 2002, **85**, 995–1001.
- 17 M. Khan, D. Lehmann and G. Heinrich, *EXPRESS Polym. Lett.*, 2008, **2**, 284–293.
- 18 F. D. B. d. Sousa and C. H. Scuracchio, *Mater. Res.*, 2015, **18**, 791–797.
- 19 H. Zhang, Z. Zhang, G. Zhao and Y. Liu, *Micro Nano Lett.*, 2016, **11**, 402–406.
- 20 S. Savetlana, H. Zuhlendri, I. Sukmana and F. A. Saputra, *IOP Conf. Ser.: Mater. Sci. Eng.*, 2017, **223**, 012009.
- 21 C. M. Long, M. A. Nascarella and P. A. Valberg, *Environ. Pollut.*, 2013, **181**, 271–286.
- 22 B. Huneau, I. Masquelier, Y. Marco, V. Le Saux, S. Noizet, C. Schiel and P. Charrier, *Rubber Chem. Technol.*, 2016, **89**, 126–141.
- 23 Y. Liu, L. Li, Q. Wang and X. Zhang, *J. Polym. Res.*, 2011, **18**, 859–867.
- 24 W. Mars and A. Fatemi, *Rubber Chem. Technol.*, 2004, **77**, 391–412.
- 25 M. Maiti, M. Bhattacharya and A. K. Bhowmick, *Rubber Chem. Technol.*, 2008, **81**, 384–469.
- 26 K. K. Sadasivuni, D. Ponnamma, S. Thomas and Y. Grohens, *Prog. Polym. Sci.*, 2014, **39**, 749–780.
- 27 L. Tzounis, S. Debnath, S. Rooj, D. Fischer, E. Mäder, A. Das, M. Stamm and G. Heinrich, *Mater. Des.*, 2014, **58**, 1–11.
- 28 A. A. Azira, M. M. Kamal and M. Rusop, *AIP Conf. Proc.*, 2016, **1733**, 020003.
- 29 A. Fakhru'l-Razi, M. A. Atieh, N. Girun, T. G. Chuah, M. El-Sadig and D. R. A. Biak, *Compos. Struct.*, 2006, **75**, 496–500.
- 30 S. Sagar, N. Iqbal, A. Maqsood and M. Bassyouni, *Int. J. Eng. Technol.*, 2014, **6**, 168–173.
- 31 P. Sae-Oui, U. Thepsuwan, P. Thaptong and C. Sirisinha, *Adv. Polym. Technol.*, 2014, **33**, 21422.
- 32 R. Brown, *Physical testing of rubber*, Springer Science & Business Media, 2006.
- 33 B. Jurkowska, B. Jurkowski, P. Kamrowski, S. S. Pesetskii, V. N. Koval, L. S. Pinchuk and Y. A. Olkhov, *J. Appl. Polym. Sci.*, 2006, **100**, 390–398.
- 34 O. A. Al-Hartomy, A. A. Al-Ghamdi, F. Al-Salamy, N. Dishovsky, D. Slavcheva and F. El-Tantawy, *Int. J. Polym. Sci.*, 2012, 1–8.
- 35 V. V. Zuev, *Macromol. Symp.*, 2011, **301**, 157–161.
- 36 V. A. Harmandaris, M. Doxastakis, V. G. Mavrantzas and D. N. Theodorou, *J. Chem. Phys.*, 2002, **116**, 436–446.
- 37 M. Doxastakis, V. G. Mavrantzas and D. N. Theodorou, *J. Chem. Phys.*, 2001, **115**, 11339–11351.
- 38 Y. Abe and P. J. Flory, *Macromolecules*, 1971, **4**, 230–237.
- 39 I. Bahar, B. Erman, F. Kremer and E. W. Fischer, *Macromolecules*, 1992, **25**, 816–825.
- 40 J. Diani, B. Fayolle and P. Gilormini, *Mol. Simul.*, 2008, **34**, 1143–1148.
- 41 D. V. Guseva, P. V. Komarov and A. V. Lyulin, *J. Chem. Phys.*, 2014, **140**, 114903.
- 42 P. Sharma, S. Roy and H. A. Karimi-Varzaneh, *J. Phys. Chem. B*, 2016, **120**, 1367–1379.
- 43 Y. N. Pandey, A. Brayton, C. Burkhart, G. J. Papakonstantopoulos and M. Doxastakis, *J. Chem. Phys.*, 2014, **140**, 054908.
- 44 Y. He and Y. Tang, *J. Theor. Comput. Chem.*, 2013, **12**, 1350011.
- 45 F. Gong, H. M. Duong and D. V. Papavassiliou, *AIP Conf. Proc.*, 2016, **1790**, 150001.
- 46 S. Y. Kwon, I. M. Kwon, Y.-G. Kim, S. Lee and Y.-S. Seo, *Carbon*, 2013, **55**, 285–290.
- 47 C.-T. Lu, A. Weerasinghe, D. Maroudas and A. Ramasubramaniam, *Sci. Rep.*, 2016, **6**, 31735.
- 48 M. J. Abraham, T. Murtola, R. Schulz, S. Páll, J. C. Smith, B. Hess and E. Lindahl, *SoftwareX*, 2015, **1**, 19–25.
- 49 M. Parrinello and A. Rahman, *J. Appl. Phys.*, 1981, **52**, 7182–7190.
- 50 G. Bussi, D. Donadio and M. Parrinello, *J. Chem. Phys.*, 2007, **126**, 014101.
- 51 T. Darden, D. York and L. Pedersen, *J. Chem. Phys.*, 1993, **98**, 10089–10092.
- 52 U. Essmann, L. Perera, M. L. Berkowitz, T. Darden, H. Lee and L. G. Pedersen, *J. Chem. Phys.*, 1995, **103**, 8577–8593.
- 53 M. Karttunen, J. Rottler, I. Vattulainen and C. Sagui, *Curr. Top. Membr.*, 2008, **60**, 49–89.

- 54 B. Hess, *J. Chem. Theory Comput.*, 2008, **4**, 116–122.
- 55 J. Wong-ekkabut, M. S. Miettinen, C. Dias and M. Karttunen, *Nat. Nanotechnol.*, 2010, **5**, 555–557.
- 56 J. Wong-ekkabut and M. Karttunen, *J. Chem. Theory Comput.*, 2012, **8**, 2905–2911.
- 57 J. Wong-ekkabut and M. Karttunen, *Biochim. Biophys. Acta, Biomembr.*, 2016, **1858**, 2529–2538.
- 58 W. Humphrey, A. Dalke and K. Schulten, *J. Mol. Graphics*, 1996, **14**, 33–38.
- 59 B. L. de Groot and H. Grubmuller, *Science*, 2001, **294**, 2353–2357.
- 60 J. Wong-ekkabut and M. Karttunen, *J. Biol. Phys.*, 2016, **42**, 133–146.
- 61 N. Michaud-Agrawal, E. J. Denning, T. B. Woolf and O. Beckstein, *J. Comput. Chem.*, 2011, **32**, 2319–2327.
- 62 A. A. Teraoka and I. Teraoka, *Polymer solutions: an introduction to physical properties*, John Wiley & Sons, 2002.
- 63 S. Fujiwara and T. Sato, *J. Chem. Phys.*, 1997, **107**, 613–622.
- 64 L. J. Fetters, D. J. Lohse and W. W. Graessley, *J. Polym. Sci., Part B: Polym. Phys.*, 1999, **37**, 1023–1033.
- 65 J. Brandrup, *Polymer Handbook*, John Wiley & Sons, Inc., New York, 4th edn, 1999.
- 66 V. Harmandaris and M. Doxastakis, *J. Chem. Phys.*, 2013, **139**, 034904.
- 67 A. Afzal, A. Kausar and M. Siddiq, *Polym.-Plast. Technol. Eng.*, 2016, **55**, 1988–2011.
- 68 C. Wei, D. Srivastava and K. J. N. L. Cho, *Nano Lett.*, 2002, **2**, 647–650.
- 69 O. V. Alekseeva, V. P. Barannikov, N. A. Bagrovskaya and A. V. Noskov, *J. Therm. Anal. Calorim.*, 2012, **109**, 1033–1038.
- 70 J. Barnoud, G. Rossi and L. Monticelli, *Phys. Rev. Lett.*, 2014, **112**, 068102.
- 71 E. Von Meerwall, J. Grigsby, D. Tomich and R. Van Antwerp, *J. Polym. Sci., Polym. Phys. Ed.*, 1982, **20**, 1037–1053.
- 72 N. Nisoh, M. Karttunen, L. Monticelli and J. Wong-ekkabut, *RSC Adv.*, 2015, **5**, 11676–11685.
- 73 J. Wong-ekkabut, S. Baoukina, W. Triampo, I. M. Tang, D. P. Tieleman and L. Monticelli, *Nat. Nanotechnol.*, 2008, **3**, 363–368.
- 74 R. C. Pani, B. D. Bond, G. Krishnan and Y. G. Yingling, *Soft Matter*, 2013, **9**, 10048–10055.
- 75 H. Ebadi-Dehaghani and M. Nazempour, *Thermal conductivity of nanoparticles filled polymers*, INTECH Open Access Publisher, 2012.